CONF-850410--33

LMFBR SOURCE TERM EXPERIMENTS IN THE FUEL AEROSOL SIMULANT TEST (FAST) FACILITY*

J. C. Petrykowski and A. W. Longest

OAK RIDGE NATIONAL LABORATORY
Oak Ridge, Tennessee 37831

CONF-850410--33

TI85 011428

Published in Proceedings of the International Topical Meeting on Fast Reactor Safety

Knoxville, Tennessee, USA

April 21-25, 1985

*Research sponsored by the Office of Nuclear Regulatory Research, U.S. Nuclear Regulatory Commission under Interagency Agreements 40-551-75 and 40-552-75 with the U.S. Department of Energy under contract DE-AC05-84OR21400 with Martin Marietta Energy Systems, Inc.

LMFBR SOURCE TERM EXPERIMENTS IN THE FUEL AEROSOL SIMULANT TEST (FAST) FACILITY

J. C. Petrykowski and A. W. Longest
OAK RIDGE NATIONAL LABORATORY
Oak Ridge, Tennessee 37831

ABSTRACT

The transport of uranium dioxide (UO_2) aerosol through liquid sodium was studied in a series of ten experiments in the Fuel Aerosol Simulant Test (FAST) facility at Oak Ridge National Laboratory (ORNL). The experiments were designed to provide a mechanistic basis for evaluating the radiological source term associated with a postulated, energetic core disruptive accident (CDA) in a liquid metal fast breeder reactor (LMFBR). Aerosol was generated by capacitor discharge vaporization of UO_2 pellets which were submerged in a sodium pool under an argon cover gas. Measurements of the pool and cover gas pressures were used to study the transport of aerosol contained by vapor bubbles within the pool. Samples of cover gas were filtered to determine the quantity of aerosol released from the pool.

The depth at which the aerosol was generated was found to be the most critical parameter affecting release. The largest release was observed in the baseline experiment where the sample was vaporized above the sodium pool. In the nine "undersodium" experiments aerosol was generated beneath the surface of the pool at depths varying from 30 to 1060 mm. The mass of aerosol released from the pool was found to be a very small fraction of the original specimen. It appears that the bulk of aerosol was contained by bubbles which collapsed within the pool.

NOMENCLATURE

h	pool level referenced to centerline of vaporizer (mm)
M	mass of aerosol in cover gas (mg) (g)
P	pressure (Pa)
R	radius of equivalent spherical bubble (mm)
V	Volume (mm^3)

Greek

α	aerosol release parameter $\equiv h_o/R_{MAX}$
γ	kinematic bubble parameter $\equiv h_o/R_{MAX}$
κ	specific heat ratio

Subscripts

B	bubble
CG	cover gas
MAX	maximum value
o	baseline value

INTRODUCTION

During low probability, energetic core disruptive accidents (CDAs) in liquid metal fast breeder reactors (LMFBRs), partially vaporized fuel and coolant could be energetically expelled from the core, forming large multiphase bubbles, displacing liquid coolant, and delivering a large impulsive load to the vessel head. The potential for release of fuel aerosol contained by the bubbles is a major concern because this aerosol represents the primary radiological source term. General statements concerning the transport and release of the fuel aerosol have remained largely speculative because of the lack of experimental data pertaining to coupled aerosol physics-bubble dynamic phenomena. Out-of-reactor experiments were recently conducted in the Fuel Aerosol Simulant Test (FAST) facility at Oak Ridge National Laboratory to study the release of uranium dioxide (UO_2) aerosols from sodium pools and to establish a data base for mechanistic assessments of the primary radiological source term associated with a CDA.

Two generic types of energetic CDAs have been postulated to release fuel, fission products, and sodium vapor from LMFBR cores (1): transient undercooling with failure to scram (TUC) and transient overpower (TOP). A TUC could be initiated by a coolant flow coastdown which would be followed by heatup and local boiling of core coolant. In a TOP, a reactivity insertion caused by rapid withdrawal of the control rods leads to fuel pin failure and mixing of molten fuel and coolant. Positive reactivity feedback in both accidents caused by sodium voiding produces a rapid power excursion and vaporization of portions of the

core. The excursions terminate when the internal core pressures are sufficient to produce mechanical disassembly. Although the fuel energy density is determined by complex reactivity feedback mechanisms, the power excursions can be characterized by a "slow" power ramp (predisassembly) followed by a "fast" power ramp (disassembly) (2).

To simulate these transients in the FAST facility, UO_2 samples were energized electrically by the capacitor discharge vaporization (CDV) technique (3) while submerged in a heated sodium pool under an argon cover gas. Joule self-heating was utilized to internally heat the samples in two stages. During the "predisassembly" stage, a controlled power supply was used to melt portions of the sample. Capacitor banks were then discharged for a few milliseconds at 10 MW levels to vaporize and disassemble the sample. During disassembly, a mixture of UO_2, xenon, and other materials expanded into the pool to form the contents of a submerged bubble. Fragmentation and condensation of UO_2 within the bubble produced aerosol during and after disassembly. The kinematics and dynamics of the bubble-pool interactions governed the transport of aerosol through the pool and the release of aerosol from the pool. Cover gas and pool pressures were measured to estimate the size of the bubble and the flow characteristics of the pool. The quantity of aerosol released from the pool was determined from chemical analysis of cover gas samples.

A series of ten experiments has been completed in which UO_2 samples were vaporized to produce aerosols of a type thought to exist following

a CDA.[1] In nine of these experiments aerosols were generated within sodium pools at depths varying from 30 to 1060 mm. The quantity of aerosol released from the pool was found to be a very small fraction of the original sample. Data are presented and analyzed here to identify conditions that affected aerosol release.

DESCRIPTION OF EXPERIMENTS

Experimental Facility

The FAST facility consists of (1) the FAST vessel and associated hardware and measurement equipment, (2) the vaporizer unit in which the UO_2 sample was initially contained, and (3) the CDV power supply system used to energize the sample. The FAST vessel and measurement equipment are shown schematically in Fig. 1. The vessel is ~1.83 m high and ~0.61 m outer diameter and has an internal volume of ~0.46 m^3. The vessel was fabricated from 0.022-m-thick 304 H stainless steel and has a removable head. The design temperature limit of the vessel is 880 K; the design pressure limit is 3.08 MPa. Electric heaters attached to the vessel were used to maintain an operating temperature of ~800 K.

The vaporizer unit, shown schematically in Fig. 2, includes two tungsten electrodes, a UO_2 sample, and sample holders. A sample consisted of 13 UO_2 pellets (4.85 mm-dia.) stacked end-to-end having a total mass of ~17.3 g and an overall length of ~90 mm. The pellet stack was surrounded by ~32 g of UO_2 microspheres [300 to 500 μm (diameter)] which were used to thermally insulate the pellets. Electrical contact

---

[1]For a description of the relevant types of aerosol in LMFBR safety studies, see the paper by Schikarski and Schuetz (5).

with the power supply was maintained through electrodes at the ends of the pellet stack. Pellets and microspheres were contained in a quartz tube which was housed within a steel tube. The gap between the tubes and the void space between microspheres were pressurized with xenon to simulate fission gases. Axial and circumferential grooves were scribed on the steel tube to provide fracture sites for efficient rupture during the capacitor discharge.

The CDV power supply system consists of a power-controlled preheater, capacitor banks, electrical connections to the vaporizer unit, and switching and control circuitry. Electric power delivered to the sample from the preheater and capacitor banks was converted to thermal energy by Joule self-heating. The preheater was used to lower the electrical resistance of the sample by several orders of magnitude to enable a very rapid (~2 ms) capacitor discharge. Four capacitor banks containing ten capacitors each were fired simultaneously on a predetermined signal. Total bank capacity is 180 kJ at 2500 V although 1950 V settings were usually selected for these experiments. Power levels typically reached ~1.6 kW during preheat and ~10 MW during discharge.

Experiments were controlled and data recording was performed in the control room.

Measurement of Experimental Parameters

Preheat measurements. Measurements were made of the electric power, the voltage drop, and the electric current supplied to the sample. During preheat an ac power supply was used, and constant power levels were maintained by conduction angle control (phase firing) of

inverse-parallel silicon-controlled rectifiers (6). Because voltage and current were in-phase, measurement of the peak values was used to calculate the sample resistance at specified preheat power levels.

The power input and resistance data were used to compute a corresponding steady-state temperature distribution in the sample (7). An iterative, finite difference technique was used to calculate heat transfer in a series of concentric cylinders (pellet stack surrounded by microspheres). Joule heating is represented by a distribution of heat sources; the total heat released by these sources balances the heat loss by radiation from the outermost microspheres. Figure 3 shows the predicted distribution for a preheat power level of 1600 W and suggests that partial melting occurred for these conditions. This conclusion was supported by Wright's preheat-only experiment (8).

The internal energy of the sample at the end of preheat could be determined from the temperature distribution and published thermophysical property data.

Capacitor discharge measurements. During capacitor discharge, measurements were made of the circuit current and the voltage drop across the test sample, cables, and shunt as a function of time after the start of capacitor discharge. These data were recorded using an oscilloscope which digitized analog input data as rapidly as 0.5 μs per point. Using a recording rate of 10 μs per point, a 10-ms record of capacitor discharge voltage and current was obtained in each experiment.

An example of the recorded capacitor discharge voltage and current data is shown in Fig. 4. The figure shows that the current rose sharply at 2.95 ms after the start of capacitor discharge, which was interpreted

as a current shunt between the high voltage electrode and ground. This occurred when sufficient UO_2 vapor had evolved to overpressurize and rupture the quartz and steel tubes and disassemble the sample. The voltage and current data were used to calculate the energy input to the sample caused by Joule heating, assuming that no significant energy input occurred after shorting began. This "CDV energy input" was calculated by time integrating the voltage-current product. Estimates of the peak energy density of the sample were made by adding the "CDV energy input" to the internal energy of preheat. As an example, the peak energy density in FAST-104 was estimated to be ~2.8 kJ/g.

Thermo-mechanical Measurements

Pressure measurements. As the sample disassembled, a dynamic multiphase mixture was formed containing UO_2 vapors and solids, xenon and perhaps, steel, quartz, and sodium. Pressures resulting from heat, mass, and momentum transfer between the mixture and the surrounding media were measured using two capacitance-type strain gage pressure transducers. One transducer was positioned radially 0.23 m from the vaporizer assembly; the other was positioned axially, above the vaporizer assembly, near the top of the vessel. In all but one experiment (FAST-111), the sodium pool covered the vaporizer and the submerged mixture formed a bubble. The radially and axially mounted transducers measured the pool and cover gas pressure, respectively. Cover gas pressure measurements were also used to estimate the size of the bubble as a function of cover gas compression.

Pressure measurements were recorded using a high speed digitizing oscilloscope. Recording rates of 50 μs/point were usually selected.

Liquid level measurements. The level of the sodium pool was adjusted in each experiment in order to vary the distance between the vaporizer and the cover gas. Since this distance was roughly equivalent to the distance a submerged aerosol particle must travel before entering the cover gas, accurate liquid level measurements were needed. An electrical resistance-type meter measured levels to within an estimated ±3 cm uncertainty in experiments 104—112. A more accurate, electrical continuity probe was used in FAST 113 because the desired liquid level (30 mm) fell within the uncertainty range of the resistance device.

Aerosol Measurements

Aerosol mass concentration measurements in the cover gas were made using an eight-port single-stage mass sampler. The sampler was installed at the top of the vessel and was connected to eight, 3-liter, pre-evacuated sampling bottles. The sampling procedure measured both the amount of argon cover gas drawn through an aerosol collection filter (located in the cover gas space) and the amount of material trapped by the filter (9-12). Sintered stainless steel (Type 316) filters measuring 28.5-mm-diam by 1.6-mm-thick with a 2-μm pore size were used. The filters were analyzed for uranium using a fluorometric technique and for sodium, silicon, iron, and other elements by inductively coupled plasma spectrometry. The amount of aerosol transported to the cover gas and the rate at which depletion occurred were determined from these data.

FAST Experimental Procedures

Each of the FAST experiments followed the same procedures. While maintaining an argon purge through the vessel, the vaporizer unit and aerosol sampling equipment were loaded into the vessel. The vessel was evacuated to reduce the residual oxygen content and was then backfilled with argon to provide an inert environment for the sodium. Sodium holding tanks and plumbing were heated above the sodium melting point so that liquid sodium flow could be initiated. Transfer of sodium to the vessel was achieved by applying argon pressure to the tanks while fill-and-drain valves were open. After transfer was completed, the vessel was further pressurized with argon and heated slowly over a 24-h period to an operating temperature of ~800 K. As this temperature was approached, heater settings were gradually lowered to establish a steady state temperature distribution. Final adjustments were made to the liquid level and argon cover gas and xenon sample pressures to account for thermal effects during heatup. The pool and cover gas pressure transducers were calibrated in situ and the capacitor discharge system was checked. After this check was completed, the vaporizer assembly was connected to the preheat and capacitor discharge system.

Preheating of the sample began at low power levels and increased in prescribed increments until a steady state temperature distribution was achieved at 500 to 600 W. Capacitor banks were charged to 1950 V in preparation for firing. After a final check of all systems was completed, the automatic firing sequence was activated. This sequence consisted of a high power level (~1600 W) preheat lasting 28 s, a 2 s delay for local thermal equilibration, followed immediately by capacitor bank firing.

Aerosol sampling in the cover gas commenced 1 to 2 min after firing and continued for nearly 1 h, at intervals of 2-15 min. After data were recorded, the sodium was drained from the vessel into the holding tanks and heating was terminated to allow the vessel to cool to ambient temperature (~60 h required for cooldown).

EXPERIMENTAL DATA RECORDS

Experimental Test Plan

The FAST experiments were conducted using a variety of cover gas and xenon sample pressures and sodium pool levels to determine what effect these parameters had on aerosol release to the cover gas. It was assumed that the pool level was the most critical experimental parameter affecting release because it alone accounts for the physical extremes: no release, corresponding to an infinitely high level and total release, corresponding to subvaporizer levels. For this reason, pool level settings spanned a wide range of values (-300 mm to +1060 mm) with increased selectivity at low, "positive" levels; the -300 mm pool level experiment was designed to gauge the aerosol yield potential of CDV. Argon pressure was varied to determine the effect of cover gas compressibility on bubble sizes, pool dynamics and aerosol release. Xenon pressure selectivity gauged the sensitivity of aerosol release to noncondensible carrier gas content. Both pressures were varied by factors of 2.5 during the series of experiments. Values of experimental parameters are listed in Table 1.

Control of electrical parameters. The amount of electric energy delivered to the sample during capacitor discharge varied with each experiment. Assuming delivery ceased when shorting occurred, CDV energy input was calculated by integrating the power input rate (voltage-current product) from the start of discharge to the time at which shorting began. Electrical measurements of vaporizer performance are listed in Table 2 and show that variations in CDV energy input are primarily caused by variations in shorting time. For example, the substantial decreases in CDV energy input observed in FAST-108 and -109 were attributed to early shorting of the vaporizer units. This tendency was reversed in subsequent experiments by decreasing preheat power levels to obtain lower sample temperatures and lower electrical conductivities at the start of discharge. These changes accounted for slower, more sustained power input, more uniform heating of the sample, and delayed shorting of the assembly. A somewhat arbitrary definition was adopted to categorize vaporizer performance. Energy input of 25 kJ or greater was considered to be a high yield discharge; inputs lower than 25 kJ were low yield. The aerosol yield from a 25 kJ discharge had been determined by Kelly et al (13) to be roughly 1 g.

Pool Pressure, Cover Gas Pressure and Bubble Size

Pool pressure and cover gas pressure traces are plotted in Fig. 5 for a low argon pressure (120 kPa) experiment. Each trace covers the first 100 ms of an experiment; this period includes capacitor discharge, vaporizer disassembly, and much of the ensuing hydrodynamic interactions. The first data point in each trace was synchronized to coincide

with capacitor bank firing. The predominant features of these traces are the distinct spikes in the pool pressure traces which are indicative of pressures caused by a pulsating bubble; the cover gas pressure traces were flat by comparison. A comparison of the pool and cover gas pressure traces identified an inverse correlation. For example, pressures measured from 0 to ≈40 ms in FAST-104 were inversely correlated; the cover gas pressure increased as the pool pressure decreased and vice-versa. Also, the lower cyclic frequencies evident in these segments of the pressure traces were clearly similar (≈25 Hz) suggesting a strong coupling between pool and cover gas pressures during the early phase of the bubble pulsation. High frequency components (300 Hz or greater) of the cover gas pressure traces were regarded as anomalous signals because they could not be correlated to any observable feature of the pool pressure traces. This suggested that the lower frequency components were indicative of pulsatile bubble behavior. On this basis, bubble pulsation frequencies were estimated to vary from ~20 Hz to 50 Hz in the FAST undersodium experiments. The duration of a complete series of bubble pulsations was assumed to be indicative of a "bubble lifetime": the elapsed time from formation to final collapse of a bubble. Estimates of bubble lifetimes were inferred by analyzing pool pressure traces. For example, a bubble lifetime of ≈100 ms was estimated from the FAST-104 pool pressure trace. This particular value is an upper bound estimate as other pool pressure traces decayed more rapidly (15).

Bubble sizes were estimated using cover gas pressure data in conjunction with the appropriate constitutive equation for the gas. Assuming liquid sodium incompressibility, the bubble underwent a simultaneous

volumetric expansion of magnitude equal to the cover gas compression. Isentropic approximations were used in this frequency range (20 to 50 Hz) with the specific heat ratio for argon given by: $\kappa = 1.67$. Bubble size measurements were standardized by calculating the radius of an equivalent spherical volume:

$$R = \left(\frac{3}{4\pi}\left\{V_{B_o} + V_{CG_o}\left[1 - (P_o/P)^{1/\kappa}_{CG}\right]\right\}\right)^{1/3} \quad (1)$$

An initial bubble volume of ~15,000 mm^3 was chosen, assuming that the xenon-UO_2 mixture initially occupied intra-assembly gaps in the vaporizer between microspheres and between the quartz and steel tube. Calculations of the maximum radius of the bubble were made using peak cover gas pressure measurements (neglecting the high frequency components) for every undersodium experiment; results are listed in Table 3.

Aerosol Data

The measurement of UO_2 aerosol mass was based on the chemical detection of uranium (U) in each cover gas sample. The mass of uranium in the entire cover gas volume was calculated by linearly proportioning it to the amount in an individual sample. The U aerosol mass content is plotted versus time in Figs. 6-7 for experiments conducted with cover gas pressures of 120 and 300 kPa, respectively. The mass equivalent of UO_2 aerosol corresponds to a 13.5% increase over values shown in these figures; 13.5% is the percent weight difference between UO_2 and U. Aerosol concentration can be determined by dividing aerosol mass by the cover gas volume. Both measures account for depletion of cover gas that occurred as a result of sampling (10, 11).

The experiments were categorized within three groups, based on the relative amount of aerosol detected in the cover gas. The groups, the basis for categorizing each group, and the experiments that compose each group are:

Group	Aerosol Mass in Cover Gas	Experiment
I	M <1 mg	FAST-104 through FAST-110, FAST-112
II	10 mg < M < 100 mg	FAST-113
III	M ~1 g	FAST-111

The quantities of aerosol detected in group I experiments were in the submilligram range and were near the lower limit of detection by chemical analysis methods. No further unfolding of data was possible within this group even though a parametric dependence on pool level and energy input was suspected. Nevertheless, the mass of aerosol released to the cover gas represented a large reduction (factors of 10^3 to 10^4) from the aerosol yield of ~1 g measured by Kelly et. al. (13) and Wright et. al. (14) in argon atmosphere CDV experiments. This reduction was confirmed in FAST sodium experiments spanning a wide range of pool levels including those in which the pool provided only a shallow covering of the vaporizer unit ($\leq$ 240 mm in half of these experiments). The best example of this phenomenon is FAST-108 in which less than 1 mg of aerosol was released through the 80 mm-thick pool layer. In this case, a partial explanation is provided by the relatively low CDV energy input which, coincidentally, reduced the anticipated aerosol yield. The bulk of evidence in this category suggested however that aerosol release

could be strongly impeded by a relatively thin (~200 mm) pool layer above the vaporizer.

The largest aerosol release was measured in FAST-111 (group III) in which the sample was vaporized above the pool. Abundant quantities (~1 g) were detected because aerosol was generated and released within the cover gas. The results agreed with previous measurements of aerosol yield (13, 14) and also provided evidence that the aerosol measurement and detection methods worked satisfactorily in a high-temperature argon-sodium environment.

The final experiment, FAST-113 (group II), was conducted with a sodium pool level of 30 mm, in an attempt to identify a threshold pool level below which aerosol release would increase dramatically. The results of this experiment were somewhat inconclusive. A preliminary analysis of the measured pressures in the sodium and the cover gas showed significant deviations from those measured in previous under-sodium experiments, suggesting markedly different bubble behavior. The confined vapor bubble underwent a single oscillation instead of several, and the cover gas pressure was more active than usual. Measurement of the level of the interface between the sodium and the cover gas by the special liquid-level probe showed repeated displacements (of this level) of 1 cm or more for a period of seconds following disassembly of the test sample. Posttest visual inspection of the surfaces of the aerosol sampling equipment revealed unusually thick deposits of material. These observations suggest that a rather vigorous exchange occurred between the sample, the sodium pool, and the cover gas, and that the aerosol sampling equipment had become contaminated by material from the pool.

Chemical analysis of aerosol samples confirmed that contamination had occurred. On average, a 40-fold increase in sodium content was detected in samples from this experiment. These data are listed in Table 4 along with data from other low pool level experiments for which aerosol release should be most comparable.

A 100-fold increase in uranium mass was also detected but subsequent analysis suggested that some of this material may have been in the form of UO_2 debris which had become suspended in the sodium pool during earlier experiments. Analysis indicated that the ratio of uranium-to-sodium mass on the filters was similar to that of the background contamination of uranium in the sodium pool ($\sim 10^{-3}$) (see Table 4). Consequently, it was not immediately clear whether UO_2 was released to the cover gas as an aerosol, a contaminant in the dispersed sodium, or as a combination of these forms.

Close examination of pressure traces suggested that significant release probably occurred during FAST-113. This conclusion was inferred by comparing cover gas pressure traces from FAST-113 and FAST-111, the oversodium experiment in which significant release was confirmed. High-level "noise" in both cover gas pressure traces was associated with turbulent mixing of the cover gas contents (which included UO_2 aerosols). Although the noise levels were similar, onset was delayed ~25 ms in FAST-113 (see Fig. 8). Delay was attributed to bubble retention in the pool during the initial growth phase. Onset at 25 ms was attributed to venting of bubble contents into the cover gas; venting may have occurred near the first maxima. In addition, an unusually flat pool pressure trace (see Fig. 9) in conjunction with delayed cover gas noise

indicated less coupling between pool and cover gas than in other under-sodium experiments, consistent with a less confined bubble pulsation.

It appears, therefore, that significant aerosol release did occur but perhaps not at the levels suggested by the data in Fig. 7 because of probable contamination of the filters by UO_2 debris.

ANALYSIS OF EXPERIMENTAL DATA

Several postulates are now proposed which are based on the relevant data presented in earlier sections of this paper and which describe the observed bubble dynamic-aerosol physics behavior. These postulates concern the mechanism by which aerosol was released from the sodium pool.

(i) Buoyant rise of the bubbles was negligible because the bubbles collapsed before significant buoyant rise could occur. Bubble lifetimes were much shorter than characteristic buoyant rise times. For example, the time to surface a 100-mm radius bubble from a depth of 1060 mm was calculated using the Davies-Taylor formula (16) to be 10 times greater than the bubble lifetime.

(ii) Pulsating bubbles near the pool surface experienced a downward deflection. Hydrodynamic theory (17-18) predicts that pulsating bubbles are propelled away from free surfaces. Blake and Gibson (18), in a study which quantified this phenomenon, showed that the bubble is deflected downward, the pool surface is deflected upward and both surfaces are severely distorted

by the end of the first pulsation (see figure 10 for example). The results suggest that bubble rise by buoyancy during the early, vigorous bubble pulsations would tend to be offset by these sinking deflections.

(iii) Aerosol concentrations in the cover gas were extremely low in group I experiments because aerosol was contained by pulsating bubbles and the bubbles remained submerged in the pool. Higher levels of aerosol were detected in experiments in which bubble venting was evident (group II) or where pool effects were not present (group III).

These postulates were used to derive an aerosol release parameter to identify those experiments for which aerosol release occurred. The parameter, α, was defined to be identically equal to Blake and Gibson's bubble parameter $\gamma = h/R_{MAX}$. The definition of α is:

$\alpha < 1$ when aerosol release is likely to occur (i.e., the bubble probably vents into the cover gas),

and

$\alpha > 1$ when aerosol release does not occur (i.e., the bubble does not vent into the cover gas.

Note that α is not an absolute indicator of aerosol release because situations can be envisioned for which these criteria do not apply. For example, $\alpha < 1$ does not ensure that release occurred unless drainage of the sodium layer above the bubble was completed during the first expansion. Also, some aerosol may be transported to the cover gas by non-condensible, xenon bubbles. Nevertheless, the conditions α describes visualize the kinematics of release and characterize bubble and aerosol behavior.

Virtually all of the aerosol data presented in Figs. 6-7 are consistent with the model just discussed. This conclusion is depicted in Fig. 11 where maximum bubble radii are plotted against pool level. Aerosol release was extremely low in every undersodium experiment except FAST-113 because the maximum transit distance of a particle was less than the vertical distance between vaporizer and pool surface; i.e., $\alpha = \gamma > 1$. It appears that a strictly-pulsating spherical bubble could not break the pool surface in any experiment except perhaps FAST-113 where the pool level was too low to confine a 130 mm radius bubble. As mentioned earlier, a significantly higher release was measured in FAST-113.

SUMMARY AND CONCLUSIONS

A series of ten experiments has been completed in which UO_2 samples were vaporized using a CDV technique to produce aerosols of a type thought to exist following a CDA. In nine of these experiments aerosols were generated within sodium pools at depths varying from 30 to 1060 mm. The quantity of aerosol released from the pool was found to be a small fraction of the aerosol yield. Depth was the most sensitive experimental parameter affecting release. The aerosol yield from CDV was measured in FAST-111 in which the sample was vaporized above the pool. Release was much lower than yield in the nine undersodium experiments which suggested that the sodium layer above the vaporizer strongly impeded aerosol release.

An analysis of bubble kinematics and dynamics identified three factors that contributed to low aerosol release in the undersodium experiments. Maximum bubble size was less than or equal to the pool level (i.e., initial bubble depth) in every experiment except FAST-113; in most cases, aerosol contained by a strictly pulsating bubble remained submerged in the pool. Secondly, bubble life times were shorter than characteristic buoyant rise times; bubbles collapsed before significant buoyant rise occurred. Finally, hydrodynamic theory predicts that pulsating bubbles are propelled away from a free surface; this effect would impede bubble rise within the pool thereby limiting release of aerosol from the pool. These findings will help provide a mechanistic data base for assessing LMFBR source terms.

ACKNOWLEDGMENT

The authors would like to acknowledge M. J. Kelly and J. M. Rochelle who designed the CDV system and A. L. Wright who developed the operating procedures that were utilized in these experiments.

This research was sponsored by the Office of Nuclear Regulatory Research, U.S. Nuclear Regulatory Commission under Interagency Agreements 40-551-75 and 40-552-72 with the U.S. Department of Energy under contract DE-AC05-840R21400 with Martin Marietta Energy Systems, Inc.

REFERENCES

1. "Analysis of Hypothetical Core Disruptive Accident (HCDA)," General Electric Company, GEAP-13921, December 1971.
2. T. S. Kress, G. W. Parker, and M. H. Fontana, "Work Plan: Transient Release from LMFBR Fuel," Oak Ridge National Laboratory, ORNL/TM-4875, September 1975.
3. M. J. Kelly, G. W. Parker, and J. M. Rochelle, "Development of the Capacitor Discharge Vaporization Technique to Produce Aerosols Formed under Conditions Postulated for Hypothetical Core Disruptive Accidents," Oak Ridge National Laboratory, ORNL/NUREG/TM-160, July 1978.
4. J. C. Petrykowski, A. W. Longest, J. M. Rochelle, and A. L. Wright, *Aerosol Release Experiments in the Fuel Aerosol Simulant Test Facility: Under Sodium Experiments*, to be published by Oak Ridge National Laboratory, ORNL/TM-9479.
5. W. O. Schikarski and W. P. Schuetz, *Nuclear Aerosols and LMFBR Source Term Analysis*, Proceedings of the LMFBR Safety Topical Meeting, Lyon Ecully, France, July 19-23, 1982.
6. K. Rush, J. M. Rochelle, and M. J. Kelly, "Power Regulator for Direct Heating of Material with Inverse Resistance-Temperature Properties, Oak Ridge National Laboratory, ORNL/NUREG/TM-450, June 1981.
7. A. L. Wright, unpublished notes, Oak Ridge National Laboratory.

8. A. L. Wright, A. M. Smith, and J. M. Rochelle, "Source Term Experiments in FAST/CRI-III," pp. 3–6 in *Aerosol Release and Transport Program Quarterly Progress Report for October–December 1981*, ed. by R. E. Adams and M. L. Tobias, Oak Ridge National Laboratory, ORNL/TM-8307, May 1982.

9. A. W. Longest, J. M. Rochelle, W. A. Bird, and C. V. Hardin, "Source Term Experiments in FAST/CRI-III," pp. 3-16 in *Aerosol Release and Transport Program Quarterly Progress Report for April–June 1983*, ed. by R. E. Adams and M. L. Tobias, Oak Ridge National Laboratory, NUREG/CR-3422, Vol. 2 (ORNL/TM-8849/V2), February 1984.

10. A. W. Longest, J. M. Rochelle, W. A. Bird, and C. V. Hardin, "Source Term Experiments in FAST/CRI-III," pp. 3-15 in *Aerosol Release and Transport Program Quarterly Progress Report for July–September 1983*, ed. by R. E. Adams and M. L. Tobias, Oak Ridge National Laboratory, NUREG/CR-3422, Vol. 3 (ORNL/TM-8849/V3), April 1984.

11. A. W. Longest, J. C. Petrykowski, J. M. Rochelle, W. A. Bird, and C. V. Hardin, "Source Term Experiments in FAST/CRI-III (Bi0476)," pp. 3-23 in *Aerosol Release and Transport Program Semiannual Progress Report for October–March 1984*, ed. by R. E. Adams and M. L. Tobias, Oak Ridge National Laboratory, NUREG/CR-3830, Vol. 1 (ORNL/TM-9217/V1), August 1984.

12. J. C. Petrykowski, A. W. Longest, W. A. Bird, J. M. Rochelie, and C. V. Hardin, "Source Term Experiments in FAST/CRI-III (B10476)," pp. 3-12 in *Aerosol Release and Transport Program Semiannual Progress Report for April–September 1984*, ed. by R. E. Adams and M. L. Tobias, Oak Ridge National Laboratory, NUREG/CR-3830, Vol. 2 (ORNL/TM-9217/V2), December 1984.

13. M. J. Kelly, T. S. Kress, G. W. Parker, J. M. Rochelle and M. H. Fontana, *Development and Application of Capacitor Discharge Vaporization Technique for Fuel Aerosol Studies*, Proc. Int. Mtg. Fast Reactor Safety and Related Physics, Chicago, IL, October 5-8, 1976.

14. A. L. Wright, A. M. Smith, J. M. Rochelle and T. S. Kress, *Fuel Aerosol Simulant Test Data Record Report: Argon Tests*, Oak Ridge National Laboratory, NUREG/CR-1123 (ORNL/NUREG/TM-365), March 1980.

15. J. C. Petrykowski and A. W. Longest, *Dynamics of Uranium Dioxide Vapor Bubbles in Sodium Pools*, to be published.

16. R. M. Davies and G. I. Taylor, *The Mechanics of Large Bubbles Rising through Extended Liquids and through Liquids in Tubes*, Proc. of the Royal Society of London, A200, 1960, 375.

17. J. R. Blake and P. Cerone, "A Note on the 'Impulse' Due to a Vapor Bubble Near a Boundary," *J. Austral. Math. Soc.* (Series B), 23, 1982, 383-93.

18. J. R. Blake and D. C. Gibson, "Growth and Collapse of a Vapor Cavity Near a Free Surface," *J. Fluid Mech* 111, 1981, 123-40.

Table 1. Experimental parameters

Experiment[a] No.	Type	Argon cover gas		Sample pressure (abs) at start of low preheat (kPa)	Sodium pool	
		Volume (m^3)	Pressure (abs) (kPa)		Volume (m^3)	Level above vaporizer centerline (mm)
FAST-103[b]	Undersodium	0.092	120	134	0.37	1050
FAST-104	Undersodium	0.090	120	133	0.37	1060
FAST-105	Undersodium	0.095	120	341	0.37	1040
FAST-106	Undersodium	0.30	120	340	0.16	240
FAST-107	Undersodium	0.32	121	341	0.14	140
FAST-108	Undersodium	0.34	120	340	0.12	80
FAST-109	Undersodium	0.33	300	341	0.13	100
FAST-110	Undersodium	0.32	300	340	0.14	140
FAST-111	Oversodium	0.45	122	341	0.014	-300
FAST-112	Undersodium	0.30	300	338	0.16	250
FAST-113	Undersodium	0.35	119	338	0.11	30

[a] In all experiments, the nominal temperatures of the vessel and the sodium were 810 K.

[b] Included for comparison. FAST-103 was performed on December 15, 1981, prior to a 1-year shutdown of the facilities.

Table 2. Electrical energy input data

Experiment No.	Preheat power[b] (W)		Resistance at end of high preheat (Ω)	Time delay between high preheat and CDV (s)	Energy stored in capacitor banks (kJ)	CDV time to shorting (ms)	CDV energy input (kJ)
	Low	High					
FAST-103[a]	600	1600	0.43	2.0	76.5	3.15	37.9
FAST-104	600	1600	0.44	2.0	76.5	3.14	37.4
FAST-105	600	1600	0.41	2.0	76.9	2.61	32.2
FAST-106	600	1600	0.41	2.0	76.9	2.98	37.6
FAST-107	600	1600	0.46	2.0	76.5	2.30	28.8
FAST-108	600	1600	0.39	2.0	76.9	1.55	19.6
FAST-109	600	1600	0.40	2.0	76.5	1.65	20.3
FAST-110	540	1600	0.40	2.0	76.5	2.35	28.2
FAST-111	500	1550	0.41	2.0	77.3	1.93	22.8
FAST-112	540	1600	0.40	2.0	76.5	2.16	26.5
FAST-113	540	1600	0.41	2.0	76.5	2.95	37.0

[a]Included for comparison. FAST-103 was performed on December 15, 1981, prior to a 1-year shutdown of the facilities.

[b]Preheat power levels modified for FAST-110 through FAST-113 to improve vaporizer performance.

Table 3. Calculated maximum bubble radius using cover gas pressure measurements

Experiment No.	R_{MAX} (mm), Eq. (1)
FAST-104	100
FAST-105	80
FAST-106	110
FAST-107	100
FAST-108	80
FAST-109	90
FAST-110	60
FAST-112	60
FAST-113	130

Table 4. A comparison of the chemical composition of aerosol samples collected in four experiments

Experiment No.	Ave. sodium content (mg)	Ave. uranium composition (wt. U/wt. Na)
FAST-108	4.00	0.56×10^{-3}
FAST-109	5.95	0.20×10^{-3}
FAST-111	5.11	1.59
FAST-113	198.0	1.9×10^{-3}

FIGURE CAPTIONS

Fig. 1. Simplified schematic of FAST vessel.

Fig. 2. FAST vaporizer unit schematic.

Fig. 3. Calculated temperature distribution in UO_2 pellets and microspheres following 1600W preheat.

Fig. 4. Measured voltage and current during a typical capacitor discharge vaporization (FAST-113).

Fig. 5. Measured cover gas pressure (upper) and pool pressure (lower), FAST-104 (baseline cover gas pressure is 120 kPa).

Fig. 6. Measured uranium mass in ~120 kPa argon cover gas (curves fitted visually).

Fig. 7. Measured uranium mass in ~300 kPa argon cover gas (curves fitted visually).

Fig. 8. Comparison of cover gas pressure traces in FAST-111 (a) and FAST-113 (b). Delayed onset of noise in FAST-113 indicates venting of bubble was retarded by layer of sodium above vaporizer.

Fig. 9. Pool pressure trace, FAST-113. The presence of a single pressure pulse indicates that venting may have occurred before the bubble collapsed.

Fig. 10. Bubble and pool surface profiles following underwater vapor explosions ($\gamma = 0.98$). Contour numbers are indexed to advancing time (see source for description). Source: reprinted with permission from J. R. Blake and D. C. Gibson, "Growth and Collapse of a Vapor Cavity Near a Free Surface," Journal of Fluid Mechanics 111, 123-140 (1981), Cambridge University Press.

Fig. 11. Position of bubble surface relative to undisturbed pool surface at closest approach. It is assumed that buoyancy and surface effects are negligible and the bubble center remains stationary. Closest approach occurs when the bubble radius is a maximum.

FILE AS ORIGINAL

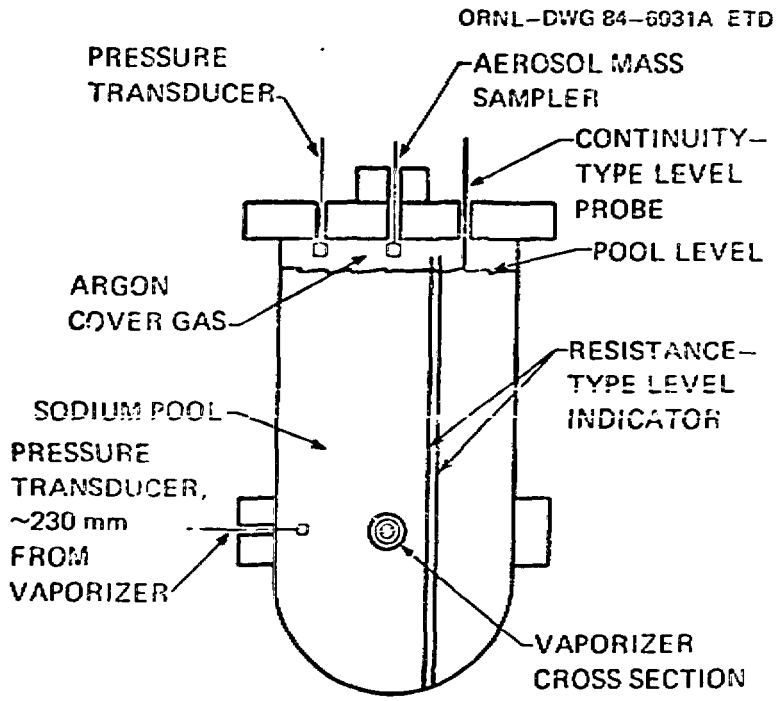

Fig. 1

FILE IS ORIGINAL

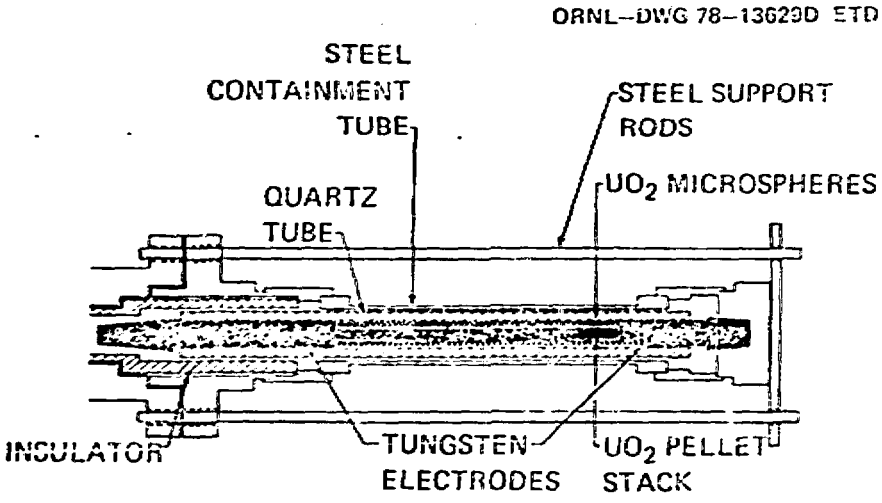

Fig. 2

FILE AS ORIGINAL

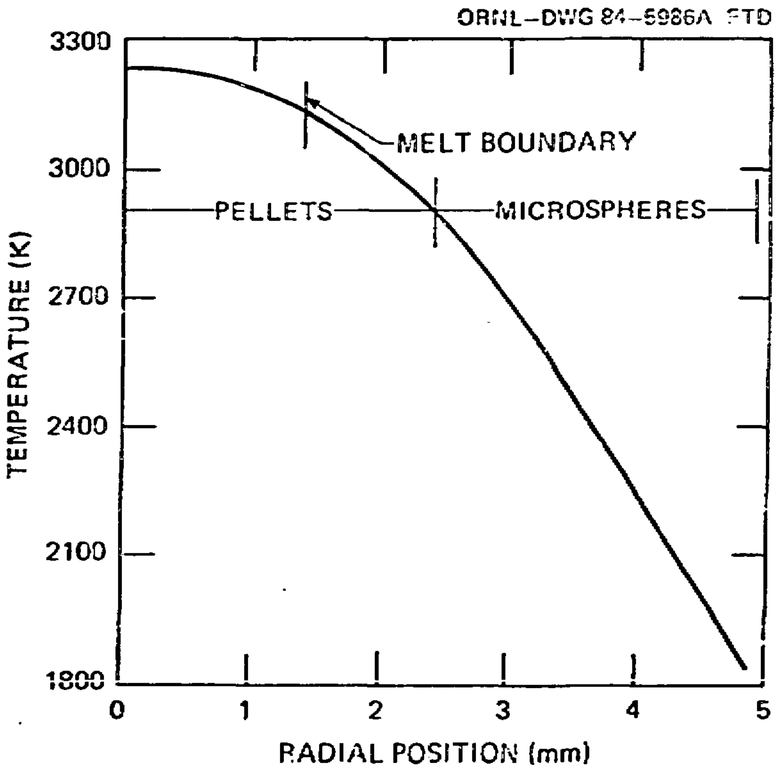

Fig. 3

FILE AS ORIGINAL

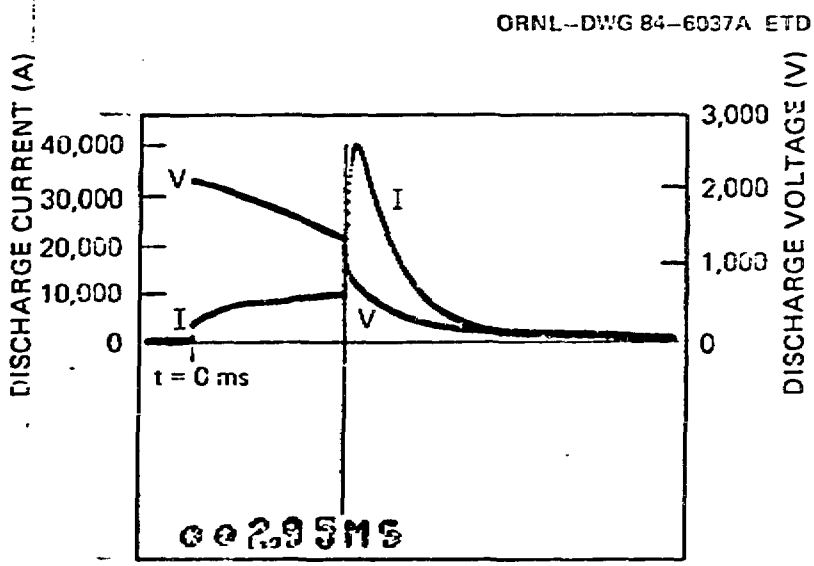

Fig.

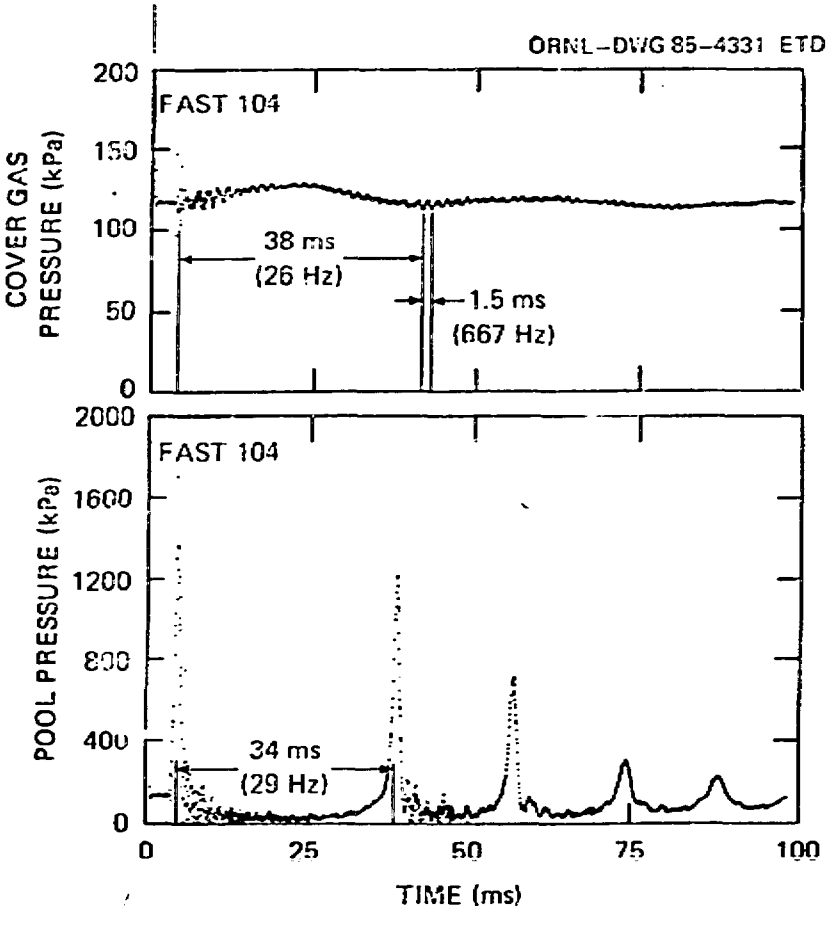
ORNL–DWG 85–4331 ETD
FAST 104
COVER GAS PRESSURE (kPa)
200
150
100
50
0
38 ms
(26 Hz)
1.5 ms
(667 Hz)
FAST 104
POOL PRESSURE (kPa)
2000
1600
1200
800
400
0
34 ms
(29 Hz)
0
25
50
75
100
TIME (ms)

FILE AS ORIGINAL

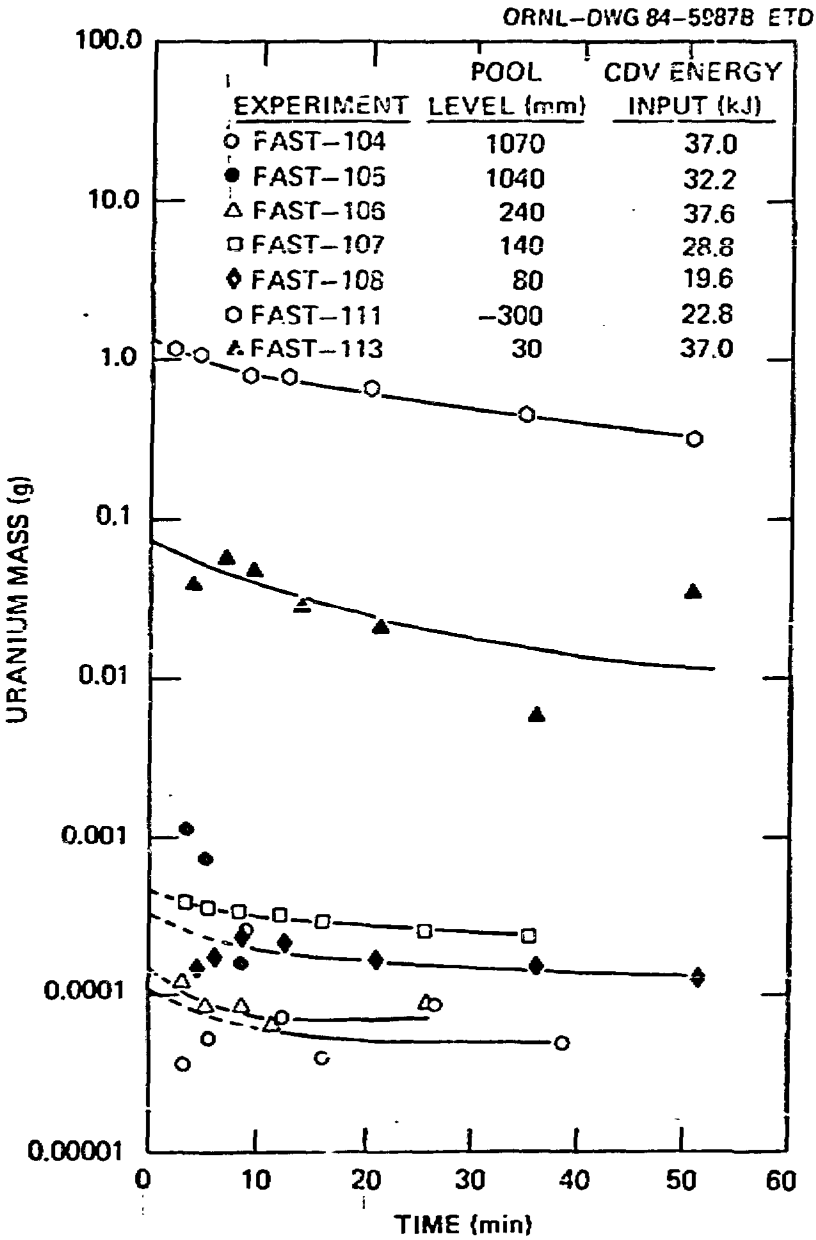

Reduce 4" to 4 1/16"

Fig.

Tetyrkowski

FILE AS ORIGINAL

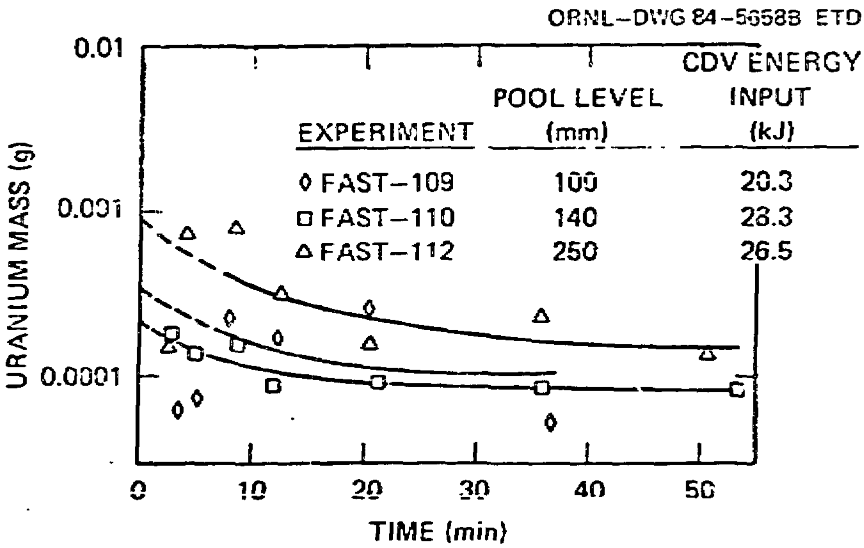

Reduce to 4"

Fig. 7

Petrykowski
Fuel-Coolant Interaction

Fig. 7

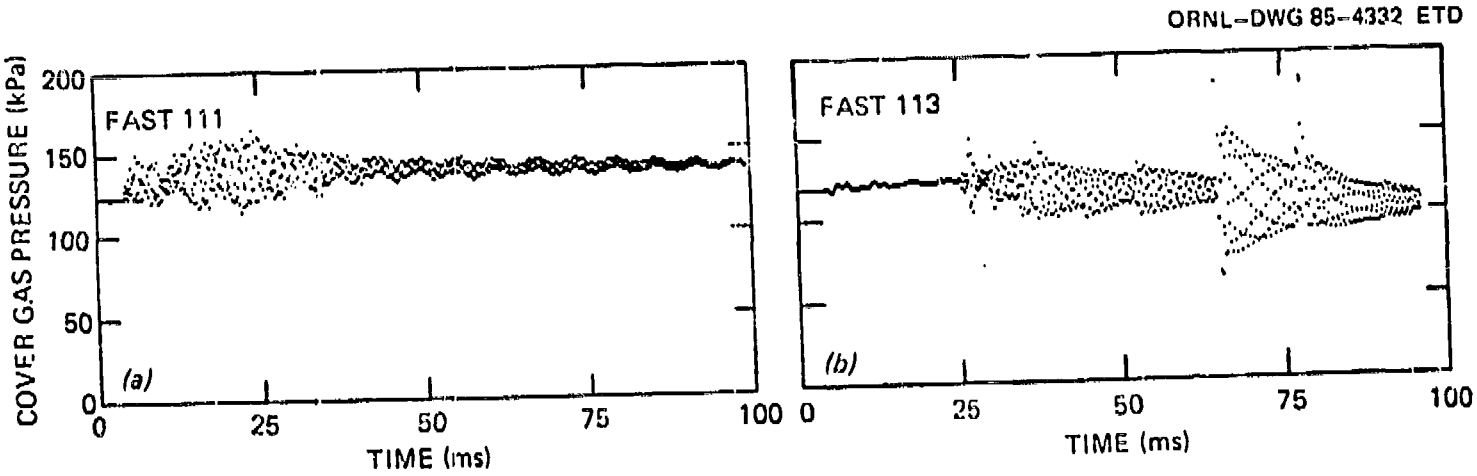
ORNL-DWG 85-4332 ETD
COVER GAS PRESSURE (kPa)
200
150
100
50
0
FAST 111
(a)
0
25
50
75
100
TIME (ms)
FAST 113
(b)
0
25
50
75
100
TIME (ms)

Fig. 3

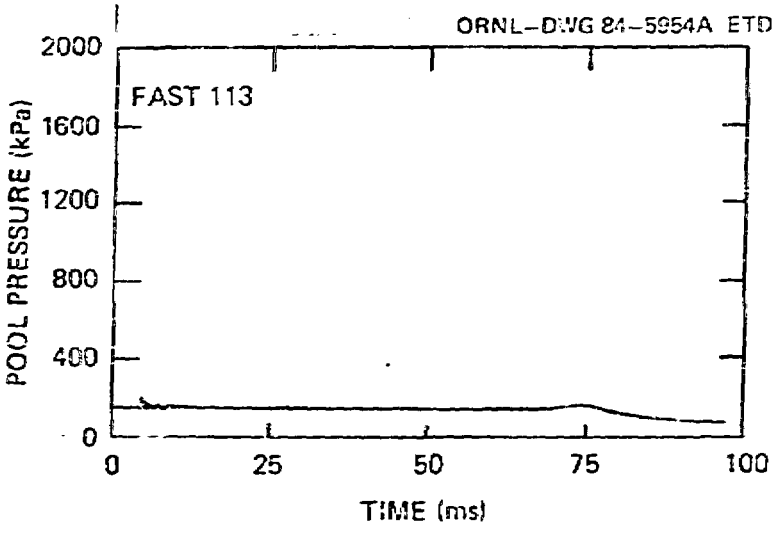
ORNL-DWG 84-5954A ETD
FAST 113
POOL PRESSURE (kPa)
2000
1600
1200
800
400
0
0
25
50
75
100
TIME (ms)

FILE AS ORIGINAL

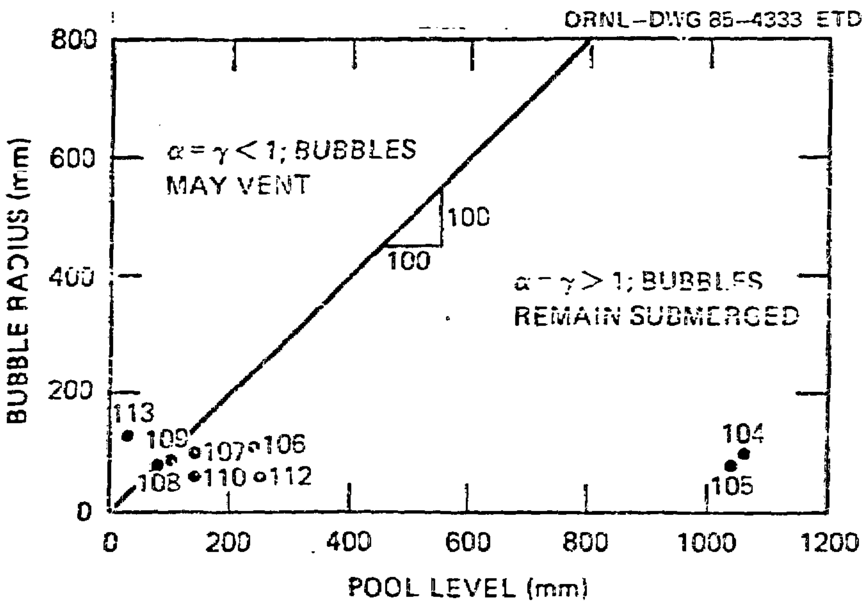

Reduce to 4" —

Fig. 11

FILE AS ORIGINAL

ORNL–DWG 84–6036A ETD

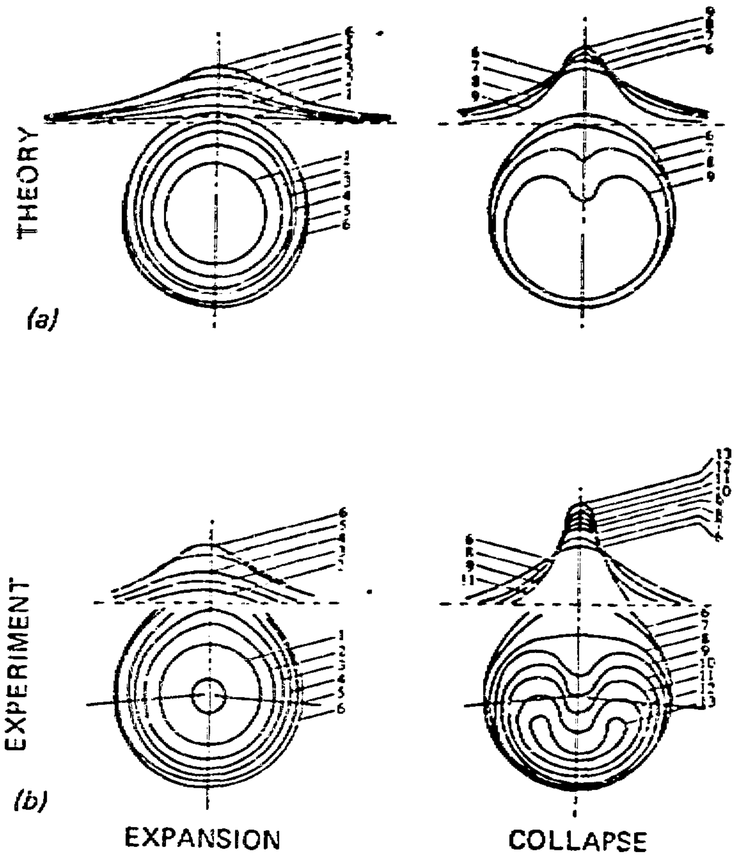

Fig. 10

Pelyakowski Fig 3. Inst. Rev. Sci. Mg. 56(1)